Journal of Alloys and Compounds 509 (2011) 627–631

Contents lists available at ScienceDirect

Journal of Alloys and Compounds

journal homepage: www.elsevier.com/locate/jallcom

The maximum solubility of Y in α-Mg and composition ranges of $Mg_{24}Y_{5-x}$ and Mg_2Y_{1-x} intermetallic phases in Mg–Y binary system

H.D. Zhao, G.W. Qin*, Y.P. Ren, W.L. Pei, D. Chen, Y. Guo

Key Laboratory for Anisotropy and Texture of Materials (Ministry of Education), Northeastern University, Wenhu Road 3-11, Heping District, Shenyang, Liaoning Province 110004, China

ARTICLE INFO

Article history:
Received 20 July 2010
Received in revised form
18 September 2010
Accepted 22 September 2010
Available online 1 October 2010

Keywords:
Mg–Y system
Diffusion couple
Solid solubility
Intermetallic compound
Phase diagram

ABSTRACT

The solid solubility of Y in the α-Mg matrix and composition homogeneity ranges of $Mg_{24}Y_{5-x}$ and Mg_2Y_{1-x} phases in the Mg–Y binary system are important parameters to understand solid–solution- and aging-strengthening effects of Mg–Y-based alloys. However, they are different among the various assessed Mg–Y phase diagrams which are based on limited experimental data, especially at temperatures below ~850 K. Our experimental results by using both diffusion couple technique and alloy method are in good agreement each other, but much different from the presently accepted Mg–Y phase diagram. The results show that the maximum solubility of Y in the α-Mg matrix is 4.7 at.% Y, much larger than the current phase diagram. The determined composition homogeneity ranges of $Mg_{24}Y_{5-x}$ and Mg_2Y_{1-x} phases are much wider than the present ones and shift remarkably to the Mg-rich corner of Mg–Y phase diagram.

1. Introduction

The Mg–Y-based alloys are important Mg-based structural materials since they have high specific strength at ambient and elevated temperatures, excellent creep resistance and good corrosion resistance as well as a considerable age hardening response [1–4]. One of the outstanding features of Mg–Y-based alloys is that they usually exhibit both solution and aging-strengthening effects during decomposition of their supersaturated solid solutions [5,6]. The effects are strongly related to solubility of Y in α-Mg matrix and volume of the intermetallic phases [7]. Therefore, the accurate determination of the Mg–Y binary phase diagram is a fundamental basis to design novel Mg–Y-based ternary and multi-component alloys and to well understand composition- and phase-dependent mechanical properties of Mg alloys.

The Mg–Y phase diagram was first determined by Gibson and Carlson [8] using thermal analysis, X-ray diffraction and microstructure analysis, later completed by Mizer and Clark [9], Miannay et al. [10], Smith et al. [11] and Sviderskaya and Padezhnova [12] using thermal analysis and/or microstructure analysis over 40 years ago. Based on the experimental information above, the Mg–Y system was first assessed by Nayeb-Hashemi and Clark [13]. The assessed diagram gave the terminal solid solution of Y in the α-Mg and amended the homogeneity ranges of ε-$Mg_{24}Y_{5-x}$ and MgY_{1-x} phases, but the δ-Mg_2Y phase was reported as a strictly line compound. And then, Giovannini et al. [14] and Flandorfer et al. [15] claimed a wide homogeneity range for δ-Mg_2Y_{1-x} phase. Fabrichnaya et al. [16] and Kang et al. [17] further thermodynamically re-assessed this binary system, which is well accepted now by most researchers in the field of Mg alloys. However, all of these works were based on very limited experimental data of $Mg_{24}Y_{5-x}$ and Mg_2Y_{1-x} phases, especially at temperatures below 850 K, making it poorly facilitate to understand the microstructures of Mg–Y-based alloys as well as their aging-strengthening effect. On the other hand, the maximum solubility of Y in the α-Mg matrix varies among different groups [11,13,15–18], and thus this variation makes it hard to well understand both solution- and aging-strengthening effects in the developed Mg–Y-based alloys.

Considering the superior properties of Mg–Y-based alloys and Mg–Y intermetallic phases playing important role in comprehensive mechanical properties, it is necessary to enrich the accurate information of Mg–Y phase diagram, especially of the solid solubility of Y in the α-Mg and composition ranges of Mg–Y intermetallic compounds below ~850 K. In this work, therefore, the solid solubility of Y in the α-Mg and the homogeneity ranges of intermetallic phases at the Mg-rich corner, $Mg_{24}Y_{5-x}$ and Mg_2Y_{1-x}, were determined by both diffusion couple technique and alloy method at

* Corresponding author. Tel.: +86 24 8368 3772; fax: +86 24 8368 6455.
E-mail address: qingw@smm.neu.edu.cn (G.W. Qin).

0925-8388/$ – see front matter © 2010 Elsevier B.V. All rights reserved.
doi:10.1016/j.jallcom.2010.09.120

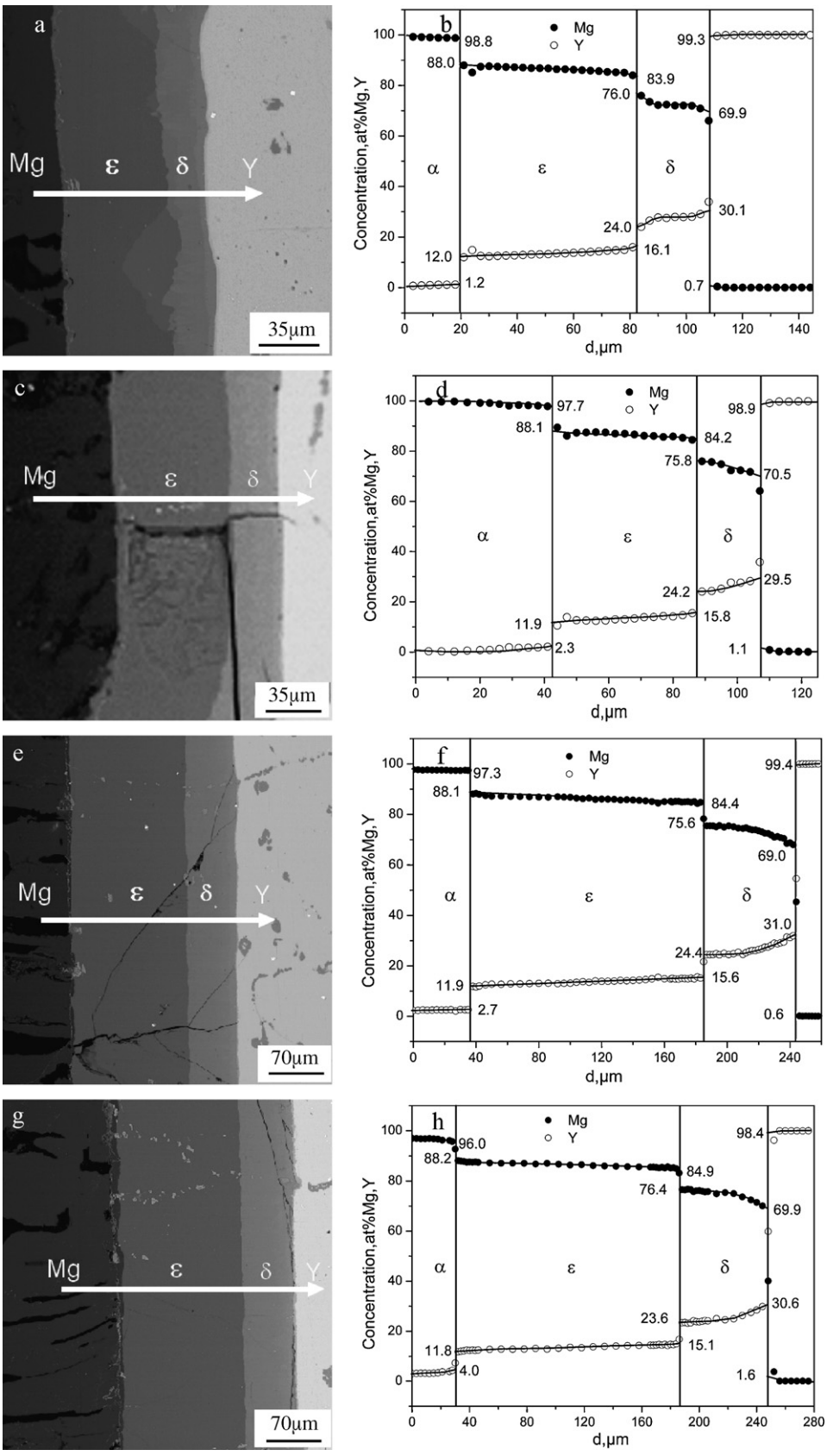

Fig. 1. Microstructures and composition profiles across the phase interfaces of the Mg/Y diffusion couples treated at different conditions: (a) and (b) 573 K for 1020 h; (c) and (d) 673 K, 900 h; (e) and (f) 723 K, 500 h; (g) and (h) 773 K, 240 h.

Table 1
Experimental data of determined phase equilibrium compositions at 573–773 K in the Mg–Y system by diffusion couple technique.

Temperature (K)	Equilibrium compositions of phase boundary (at.% Y)				
	α-Mg	ε-$Mg_{24}Y_{5-x}$		δ-Mg_2Y_{1-x}	
573	1.2	12.0	16.1	24.0	30.1
673	2.3	11.9	15.8	24.2	29.5
723	2.7	11.9	15.6	24.5	31.0
773	4.0	11.8	15.1	23.6	30.6

573–773 K. The results show much difference from the presently accepted Mg–Y binary phase diagram.

2. Experimental procedure

The cuboid-shaped specimens of 6 mm × 8 mm × 10 mm were cut from the Mg and Y raw materials (Mg: 99.99 wt.% and Y: 99.99 wt.% in purity). And then the Mg and Y specimens were pressed with a fastener, sealed in an evacuated quartz capsule, followed by diffusion welding at 573 K for one hour. Subsequently, the prepared diffusion couples were re-sealed in the quartz capsules in argon atmosphere and equilibrium at 573, 673, 723 and 773 K for 1020, 900, 500 and 240 h, respectively. After the heat treatment, the diffusion couples were subsequently quenched into water. The Mg–21 at.% Y alloy was supplied by Changchun Institute of Applied Chemistry (Chinese Academy of Science). The samples were wrapped in tantalum sheets, and sealed in evacuated quartz tubes for equilibrium treatment at 573, 673, 723 and 773 K for 3000, 2020, 900 and 68 h, respectively, and then followed by water quenching to room temperature. All the specimens of diffusion couples and alloys were mechanically grounded and polished, and their microstructure and composition analysis were examined by electron probe micro-analyzer (EPMA) (Shimadzu EPM-1610) with wavelength disperse detector under an accelerating voltage of 15 kV and a spot size of 1 μm. The ZAF program was used to calibrate the composition of each element at every detected point with the standard samples of high-purity Mg and Y. Moreover, the concentration profiles in each diffusion couple were measured and then extrapolated to the phase interfaces, and finally the equilibrium phase compositions were obtained.

The phase constituents of the heat treated Mg–21 at.% Y alloy were determined by X-ray diffraction (XRD) (PANALYTICAl B.V PW3040/60) with Cu Kα irradiation at 40 kV and 40 mA with a scanning rate of 4°/min.

3. Results and discussion

The microstructures of Mg/Y diffusion couples heat treated at 573–773 K are similar, and Fig. 1 shows the backscattered electron (BSE) image and the corresponding concentration profile across the phase interfaces of the Mg/Y diffusion couple heat treated at 573 K for 1020 h. The result shows that the three interfaces exist in the diffusion couple (Fig. 1a), which indicates that four phases are formed in this couple. The thickness of the layers varies from about 30 μm to 70 μm. The composition profiles of Mg/Y diffusion couple annealed at 573 K are illustrated in Fig. 1b. There are obviously compositional jumps at the phase interfaces. The equilibrium compositions were determined by extrapolating the composition–penetration profile to the interface boundary. The composition homogeneity ranges were determined to be 12.0–16.1 at.% Y for the ε-$Mg_{24}Y_{5-x}$ phase and 24.0–30.1 at.% Y for the δ-Mg_2Y_{1-x} phase at 573 K, respectively. Meanwhile, the solubility of Y in the α-Mg at this temperature is 1.2 at.%.

By the same token, the Mg/Y diffusion couples at the other three temperatures were determined, too. The BSE images of the diffusion couples annealed at 673 K for 900 h, 723 K for 500 h, 773 K for 240 h and the corresponding composition profiles are also shown in Fig. 1. The microstructure is similar to that in Fig. 1a, except that the thickness of diffusion layers increase with increasing annealed temperature, reached about 60–150 μm. The $Mg_{24}Y_{5-x}$ and Mg_2Y_{1-x} phases were also confirmed. All the phase equilibrium compositions obtained by the diffusion couple technique are summarized in Table 1, and marked in the Mg–Y binary phase diagram, as shown in Fig. 2.

Table 2
The equilibrium compositions of Mg–21.% Y alloy at 573–773 K in the Mg–Y system.

Treated conditions	Equilibrium compositions			
	ε-$Mg_{24}Y_{5-x}$		δ-Mg_2Y_{1-x}	
	Mg	Y	Mg	Y
573 K, 3000 h	83.2	16.8	75.1	24.9
673 K, 2020 h	84.3	15.7	76.6	23.4
723 K, 900 h	84.7	15.3	76.7	23.3
773 K, 68 h	84.8	15.2	76.9	23.1

However, the Mg–Y binary phase diagram [16] shows that there is MgY_{1-x} intermetallic phase in equilibrium with the δ-Mg_2Y_{1-x} and α-Y. Unfortunately, the diffusion layer of this phase could not be observed by SEM, probably due to very slow growth and thus too narrow to be found. This "phase loss" phenomena usually happens in a diffusion couple with a large difference in compositions between the two master alloys. The confirmation work is still in progress.

From Fig. 2, one can know the composition ranges of $Mg_{24}Y_{5-x}$ and Mg_2Y_{1-x} phases shift obviously to the Mg-rich corner, and become much larger than the presently accepted Mg–Y phase diagram. In order to confirm it, the alloy method was also used to clarify the rationality of this difference. Fig. 3b shows the microstructures (BSE images) of Mg–21 at.%Y alloy annealed at 673 K for 2020 h. The Mg–21 at.% Y alloy locates at the two phase region of $Mg_{24}Y_{5-x}$ and Mg_2Y_{1-x} in the Mg–Y binary phase diagram [16]. However, there existed three phases heat treated Mg–21 at.% Y alloy at 673 K for 900 h, as shown in Fig. 3a. Composition analysis indicates that the light phase is δ-Mg_2Y_{1-x} phase, the dark one is ε-$Mg_{24}Y_{5-x}$ phase, and the gray one is metastable ε′-$Mg_{24}Y_{5-x}$ phase with a composition of ~Mg–20.5 at.% Y. The similar results of metastable compound Mg_5Y had been reported earlier [18,19]. When the heat treatment time at 673 K reached 2020 h, the gray metastable ε′-$Mg_{24}Y_{5-x}$ phase disappeared, as shown in Fig. 3b. According to the principle of the BSE image, the dark phase is the $Mg_{24}Y_{5-x}$ phase and the light one is Mg_2Y_{1-x} phase, which is also confirmed by SEM-EDX. The other treated samples at 573, 723 or 773 K show the similar microstructures as Fig. 3b. All the phase equilibrium compositions, determined by EPMA, are summarized in Table 2, and marked in the Mg–Y phase diagram, as shown in Fig. 2.

The XRD results of the Mg–21 at.% Y alloy in the different treated conditions above do not show any significant difference, as shown in Fig. 4, composed of only $Mg_{24}Y_{5-x}$ and

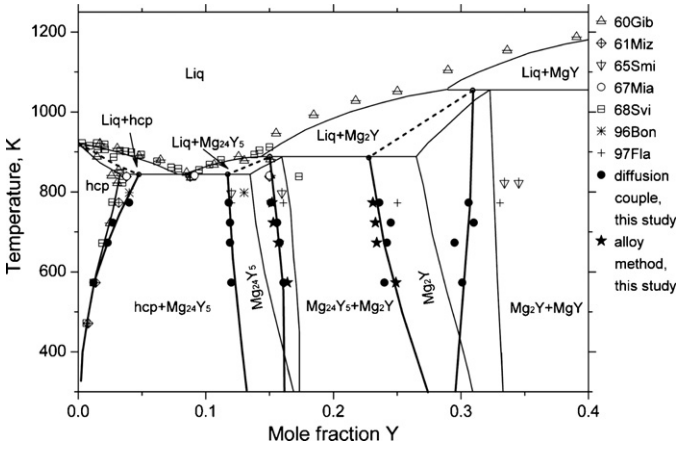

Fig. 2. Revised Mg–Y phase diagram, incorporated the experimental data of this study, together with the presently accepted assessed phase diagram and previous data.

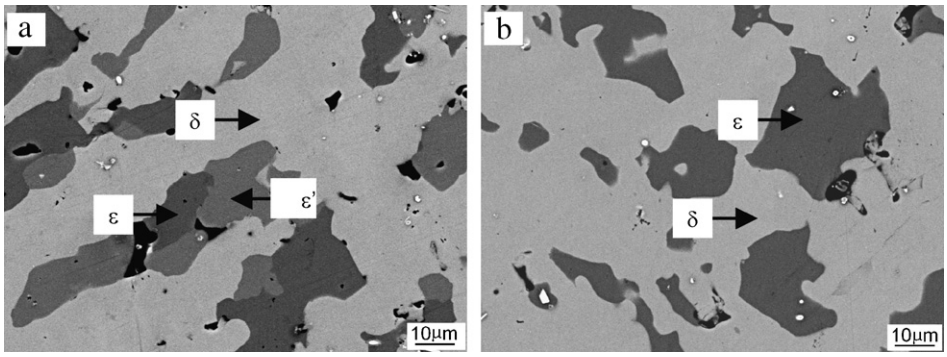

Fig. 3. Microstructures of Mg–21 at.% Y alloy annealed at 673 K for (a) 900 h and (b) 2020 h.

Mg_2Y_{1-x} phases, which is in good agreement with SEM observation.

Base on the experimental data of the diffusion couples technique and equilibrium alloy method mentioned above, the solubility of Y in the α-Mg, and the different solid solution ranges of the $Mg_{24}Y_{5-x}$ and Mg_2Y_{1-x} intermetallic phases have been obtained, as shown in Fig. 2. In this work, the solubility of Y in the α-Mg phase are determined to be 1.3–2.7 at.% Y at 573–723 K, which is in good agreement with the other experimental and assessed results [8,9,12], implying the local equilibrium in the diffusion couple samples are attained by such a long annealing time. However, the solubility of Y in the α-Mg phase goes up to ~4 at.% at 773 K determined by EPMA in this study, which is higher than that in the present Mg–Y phase diagram [8,9,12]. Bonhomme and Yvon [20] reported that the Mg–12 at.% Y alloy was annealed at 798 K for two weeks and the secondary phase was a solid solution of approximate composition Mg–4 at.% Y, which is consistent with our result. It thus suggests that sufficient long annealing time is important for alloy method to determine equilibrium phase compositions. In this case, if the solubility of Y in the α-Mg extends to the eutectic temperature, the maximum solubility is 4.7 at.% Y in the α-Mg phase, which is ~1.3 at.% Y (or ~4.6 wt.% Y) higher than the presently accepted one. As it is well known, solid solution strengthening (SSS) effect of RE is one of most effective strengthening mechanisms for Mg alloys [6,7], and it is commonly believed that Y element has much more effective SSS than Al and Mn [21]. In this study, much wider solubility range of Y in the α-Mg phase was detected, especially over 773 K, and it is thus expected the more strengthening effect of Mg–Y-based alloy could be achieved by proper solid solution treatment, and a more aging-strengthening effect could be obtained by the $Mg_{24}Y_{5-x}$ phase.

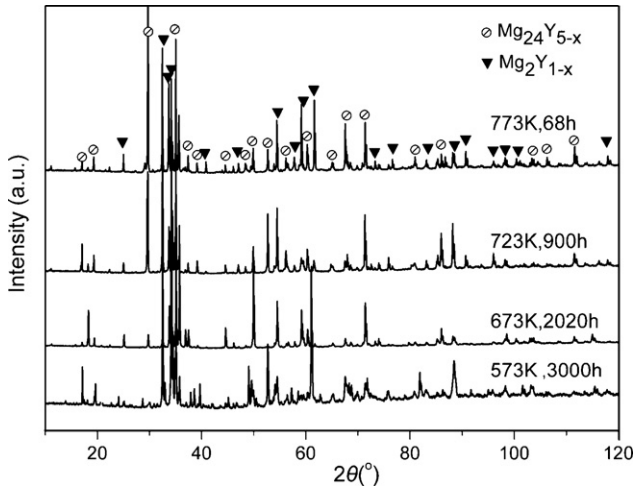

Fig. 4. XRD patterns of the Mg–21 at.% Y alloy heat treated at 573–773 K for sufficiently long time.

As to intermetallic phases of $Mg_{24}Y_{5-x}$ and Mg_2Y_{1-x}, they were early reported as stoichiometric compounds as $Mg_{17}Y_5$ and Mg_5Y_2 by means of metallography method [8,9], then Smith et al. [11] claimed they should be $Mg_{24}Y_{5-x}$ and Mg_2Y_{1-x} with a composition range of 12.5–16.0 at.% Y for $Mg_{24}Y_{5-x}$ phase and 33.2–34.2 at.% Y for Mg_2Y_{1-x} phase. Later, many other groups determined their composition ranges in the temperature range of 773–850 K, and varied one another due to not sufficient annealing time [10,11,15,16]. But there have been no experimental data below 773 K so far. In this work, we used both diffusion couple technique and alloy method to systematically determine the composition ranges of $Mg_{24}Y_{5-x}$ and Mg_2Y_{1-x} phases, and got well self-consistent results. The two single-phase regions obviously shift to the Mg-rich corner and much wider than that in the current Mg–Y phase diagram, as shown in Fig. 2. The merit of these results, especially of the maximum solubility of Y in the α-Mg and the composition range of $Mg_{24}Y_{5-x}$ phase, is to provide important information for the design of novel Mg–Y-based alloys through controlling the proper volume of precipitates.

The strengthening effects of RE, such as Y, Gd and Dy, have been explained by two mechanisms [5], one is solid solution strengthening and the other is precipitation hardening. Addition of Y in magnesium generally reduces the axis ratio [22], therefore, yttrium may change the relative activity of the deformation mode of magnesium at room temperature, resulting in the enhanced compressive ductility of extruded Mg–Y alloys over the extruded pure magnesium. The recent research by Wu et al. [23] shows that the elongation-to-failure δ increased from 15.0% to 30.0% as yttrium content increased to 4 wt.%, and this is mainly due to the different textures that make the difference of deformation modes along extruded direction for Mg–Y alloys. However it is also believed that solid solution of yttrium is one way to strengthen magnesium because of the difference in the atomic radius between yttrium and magnesium. The results of Gao et al. [3] showed that the hardness and yield strength of the Mg–Y single phase alloys increase evidently with the increasing yttrium addition of 0.2–1.88 at.% at room temperature, therefore, the yttrium addition exhibit a high solid solution strengthening effect. It is commonly believed that yttrium is an effective solid solution hardener for Mg and Mg alloys because of its wide range of solubility.

The creep resistance of magnesium is also significantly improved by the addition of yttrium even in a dilute concentration range. The addition of yttrium in magnesium alloys is more effective for strengthening than aluminum, manganese and zinc [1,6,24]. The effect of yttrium content on the mechanical properties of the other Mg alloys, such as Mg–Zr and Mg–Zn alloy, has also been studied in recent years. The tensile strength and elon-

gation of as-cast Mg–0.6%Zr based alloys could be increased with increasing yttrium content. The mechanism of improved mechanical properties is due to the refinement of α-Mg grains and solid solution strengthening by yttrium [25]. When the yttrium was added in the Mg–Zn alloy, the I-phase Mg_3YZn_6 distributed within the Mg matrix of the extruded Mg–Zn–Y alloy. These I-phase particles inhibit the grain growth during extrusion, and thus the high strength has been achieved in this alloy [26]. In this study, the larger solid solution range of Y in the α-Mg phase than previous results has been determined, and different composition ranges of $Mg_{24}Y_{5-x}$ and Mg_2Y_{1-x} phases have clarified, so the outstanding strengthening and thus precipitation effects can be expected in the Mg–Y-based alloys.

4. Conclusion

In summary, the equilibrium phase relations and phase compositions in the Mg–Y binary system were experimentally determined by means of Mg/Y diffusion couple technique and alloy method at 573–773 K. The results show that the maximum solubility of Y in the α-Mg matrix is 4.7 at.% Y, much higher than the current phase diagram. The determined composition homogeneity ranges of $Mg_{24}Y_{5-x}$ and Mg_2Y_{1-x} phases shift remarkably to the Mg-rich corner of Mg–Y phase diagram, that is, 12.0–16.1 at.% Y, 11.9–15.8 at.% Y, 11.9–15.6 at.% Y and 11.8–15.1 at.% Y for the $Mg_{24}Y_{5-x}$ phase at 573–773 K, and 24.0–30.1 at.% Y, 24.2–29.5 at.% Y, 24.5–31.0 at.% Y and 23.6–30.1 at.% Y for the Mg_2Y_{1-x} phase at 573–773 K, respectively. Based on the modification of the α-Mg, $Mg_{24}Y_{5-x}$ and Mg_2Y_{1-x} phase regions, the new phase diagram of Mg–Y system at the Mg-rich corner was thus re-constructed.

Acknowledgements

This work was supported by Key Project of National Natural Science Foundation of China (No. 50731002), the Fundamental Research Funds for the Central Universities (Nos. N090502002 and N090602004), Key Laboratory Project of Liaoning Province (No. 2008S089) and Shenyang Talents Supporting Project (No. 2007010303025).

References

[1] M. Suzuki, H. Sato, K. Maruyama, H. Oikawa, Mater. Sci. Eng. A 319–321 (2001) 751–755.
[2] L.L. Rokhlin, N.I. Nikitina, J. Alloy Compd. 279 (1998) 166–170.
[3] L. Gao, R.S. Chen, E.H. Han, J. Alloy Compd. 472 (2009) 234–240.
[4] X.M. Wang, X.Q. Zeng, Y. Zhou, G.S. Wu, S.S. Yao, Y.J. Lai, J. Alloy Compd. 460 (2008) 368–374.
[5] K. Maruyama, M. Suzuki, H. Sato, Metall. Mater. Trans. A 33 (2002) 875–882.
[6] M. Suzuki, H. Sato, K. Maruyama, H. Oikawa, Mater. Sci. Eng. A 252 (1998) 248–255.
[7] L.L. Rokhlin, N.I. Nikitina, J. Alloys Compd. 279 (1998) 166–170.
[8] E.D. Gibson, O.N. Carlson, Trans. ASM 52 (1960) 1084–1096.
[9] D. Mizer, J.B. Clark, Trans. Met. Soc. AIME 221 (1961) 207–208.
[10] D. Miannay, P. Gregoire, P. Azou, P. Bastein, Compt. Rend. 265C (1967) 1107–1112.
[11] J.F. Smith, D.M. Bailey, D.B. Novotny, J.E. Davison, Acta Metall. 13 (1965) 889–895.
[12] Z.A. Sviderskaya, E.M. Padezhnova, Izv. Akad. Nauk SSSR Met. 6 (1968) 183–190.
[13] A.A. Nayeb-Hashemi, J.B. Clark, Binary Alloy Phase Diagram (1988) 2566.
[14] M. Giovannini, R. Marazza, A. Saccone, R. Ferro, J. Alloy Compd. 203 (1994) 177–180.
[15] H. Flandorfer, M. Giovannini, A. Saccone, P. Rogl, R. Ferro, Metall. Mater. Trans. A 28 (1997) 265–276.
[16] O.B. Fabrichnaya, H.L. Lukas, G. Effenberg, F. Aldinger, Intermetallics 11 (2003) 1183–1188.
[17] Y.B. Kang, A.D. Pelton, P. Chartrand, P. Spencer, C.D. Fuerst, J. Phase Equilib. Diff. 28 (2007) 342–354.
[18] K.P. Anderko, E.J. Klimek, D.W. Levinson, Trans. ASM 49 (1957) 778–791.
[19] N.F. Lashko, G.I. Morozova, L.P. Nefedova, E.M. Nikolskaya, Izv. Akad. Nauk. SSSR. Metall. 6 (1974) 217–220.
[20] F. Bonhomme, K. Yvon, J. Alloy Compd. 232 (1996) 271–273.
[21] B.L. Mordike, Mater. Sci. Eng. A 324 (2002) 103–112.
[22] S.R. Agnew, M.H. Yoo, C.N. Tome, Acta Mater. 49 (2001) 4277–4289.
[23] B.L. Wu, Y.H. Zhao, X.H. Du, Y.D. Zhang, F. Wagner, C. Esling, Mater. Sci. Eng. A 527 (2010) 4334–4340.
[24] L. Gao, R.S. Chen, E.H. Han, J. Alloy Compd. 481 (2009) 379–384.
[25] D.Q. Wan, J.C. Wang, G.C. Yang, Mater. Sci. Eng. A 517 (2009) 114–117.
[26] X.H. Shao, Z.Q. Yang, X.L. Ma, Acta Mater. 58 (2010) 4760–4771.